Polyhedron 155 (2018) 34–41

Contents lists available at ScienceDirect

Polyhedron

journal homepage: www.elsevier.com/locate/poly

# Family of $[Ln_4Mn_8]$ (Ln = Gd, Tb, Dy, Ho) and $Y_4Mn_8$ single-molecule magnets from the use of 2-(pyridine-2-yl)propan-2-ol

Linh Pham [a,b], Khalil A. Abboud [a], Wolfgang Wernsdorfer [c], George Christou [a,*]

[a] Department of Chemistry, University of Florida, Gainesville, FL 32611-7200, USA
[b] Department of Science and Mathematics, Texas A&M University-Central Texas, Killeen, TX 76549, USA
[c] CNRS and Université Grenoble Alpes, Institut Néel, 38042 Grenoble, France

ARTICLE INFO

*Article history:*
Received 18 April 2018
Accepted 6 July 2018
Available online 29 August 2018

Dedicated to Professor Spyros Perlepes on the occasion of his 65th birthday. A great scientist and friend.

*Keywords:*
Single-molecule magnets
Manganese
Lanthanides
Magnetic properties
Heterometallic 3d–4f clusters

ABSTRACT

The syntheses, structures and magnetic properties are reported of a new family of $[Ln_4Mn_8O_8(O_2CPh)_{16}(dmhmp)_4]$ (Ln = Gd (**1**), Tb (**2**), Dy (**3**), Ho (**4**)) complexes obtained from the use in Mn–Ln chemistry of 2-(pyridine-2-yl)propan-2-ol (dmhmpH), a bulkier derivative of 2-(hydroxymethyl)pyridine (hmpH) containing a $CMe_2OH$ arm instead of $CH_2OH$. Complexes **1**–**4** were obtained from the reaction of $Mn(O_2CPh)_2$, $Ln(NO_3)_3$, dmhmpH and $NEt_3$ in a 2:1:2:4 molar ratio in MeCN/MeOH (24:2 mL), and the corresponding reaction with $Y(NO_3)_3$ gave $[Y_4Mn_8O_8(O_2CPh)_{16}(dmhmp)_4]$ (**5**). The crystal structures of representative complexes **1** and **5** were solved and they are isostructural, with centrosymmetric structures comprising five metal-containing layers in an **ABCBA** arrangement, with **A** = Gd(Y), **B** = $Mn_2Gd(Y)$, and **C** = $Mn_4$. Variable-temperature, solid-state dc and ac magnetic susceptibility studies on **1**–**5** revealed dominant antiferromagnetic interactions between the $Mn_8$ unit and the $Ln^{III}$ ions. The data for **5** ostensibly indicated a well-isolated singly-degenerate ground state, but further studies suggested instead that the ground state is an $S = 5$ state that is near-degenerate with one or more states with $S \leq 4$. Frequency-dependent ac in-phase $\chi'_M T$ and out-of-phase $\chi''_M$ signals indicate **3** (Dy) to possibly be an SMM, and this was confirmed by observation of hysteresis loops below 1.6 K in magnetization versus dc field scans below 2 K.



## 1. Introduction

Polynuclear 3d–4f complexes have inspired much interest because of their often aesthetically-pleasing structures and their intriguing electronic and magnetic properties [1–17]. Since the breakthrough in 2004 with the report of a $Tb_2Cu_2$ SMM [2], which provided proof-of-feasibility that amalgamation of transition metals with anisotropic $Ln^{III}$ ions could lead to magnetically interesting new molecules and SMMs, a wealth of new studies were initiated with various 3d–4f metal combinations. In particular, manganese-lanthanide clusters proved a rich source of single-molecule magnets (SMMs), including $[Mn_2Dy_2]$ [4], $[Mn_4Tb_2]$ [18], $[Mn_4Dy_4]$ [19], $[Mn_8Dy_4]$ [20], $[Mn_{11}Dy_4]$ [21], $[Mn_6Dy_6]$ [22], $[Mn_{11}Gd_2]$ [23], $[Mn_{12}Gd]$ [24], $[Mn_{18}Dy]$ [25], $[Mn_{21}Dy]$ [26], $[Mn_7Er]$ [27], $[Mn_{12}Tb_6]$ [28], $[Mn_{11}Dy]$ [29], $[Mn_{12}Ln_6]$ [30], $[Mn_2Ln_3]$ [31], $[Mn_3Dy_4]$ [32], $[Mn_8Dy_4]$ [33], $[MnDy_2]$ [34], $[Mn_2Dy_2]$ [35], and $[Mn_4Nd_2]$ [36]. Such molecules display both conventional hysteresis in magnetization versus dc field scans and quantum tunneling of magnetization (QTM), and they therefore represent a rare family of compounds that straddle the classical/quantum interface [4,37–42]. Very recently, a mononuclear organometallic Dy SMM which possesses a record magnetization blocking temperature of 60 K [43,44] undoubtedly represents an exciting new phase of SMM research and its applications.

The satisfying health and progress over many years of the SMM field have been primarily due to the development of many new synthetic methods that have provided a reliable supply of new materials and thus kept the field advancing. Numerous reaction conditions and ligand types have been employed with great success, followed by using the molecular advantages of monodispersity, solubility, and crystallinity to characterize the products by single-crystal X-ray crystallography. This development of new synthetic strategies has been an area in which our own group has been very much involved. One approach among many that we have employed widely has been the use of mixed N/O chelate ligands containing one or more alcohol groups whose deprotonation provides bridging alkoxides that foster higher nuclearity products. We began this approach in Mn chemistry many years ago with 2-(hydroxymethyl)pyridine (hmpH) [14,45], which has proved to

* Corresponding author.
*E-mail address:* christou@chem.ufl.edu (G. Christou).

https://doi.org/10.1016/j.poly.2018.07.007
0277-5387/

be one of the most successful ligands in the SMM field [33,46–51], and related 2,6-bis(hydroxymethyl)pyridine ($pdmH_2$) [3]. We also introduced modifications to hmpH by replacing the $CH_2$ with $CMe_2$ or $CPh_2$ groups to explore the effect of the increasing bulk near the alkoxide on the identity of the obtained $Mn_x$ cluster. These derivatives, 2-(pyridine-2-yl)propan-2-ol (dmhmpH) and diphenyl(pyridine-2-yl)methanol (dphmpH), are also very appealing ligands for synthesizing new SMMs, and a number of very interesting new products were obtained [49–51].

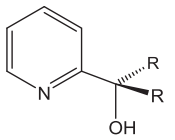


R = H is hmpH; R = Me is dmhmpH; R = Ph is dphmpH

The present work is part of the extension of the use of hmpH and its bulkier derivatives into mixed Mn-4f chemistry. This subarea began with the synthesis of the non-carboxylate $[Ln_2Mn_2(OH)_2(NO_3)_4(hmp)_4(H_2O)_4](NO_3)_2$ family [5,6,52] followed by $Ln_4Mn_2$ [53] and $Ln_2Mn_4$ [54] carboxylate clusters. More recently, $Ln_4Mn_8$ and additional $Mn_4Ln_2$ have been reported [33,55]. We herein report the products from the use of dmhmpH in this chemistry, which has yielded a family of $Ln^{III}_4Mn^{III}_8$ (**1**–**4**) and $Y^{III}_4Mn^{III}_8$ (**5**) complexes. We have obtained the crystal structures of the Gd (**1**) and Y (**5**) members, and measured the dc and ac magnetic susceptibilities of all the members of the family, which has also identified some of them to be new SMMs. We shall also describe the results obtained from a single-crystal study of the Dy analogue at ultra-low temperatures using a micro-SQUID, which has confirmed the magnetization hysteretic behavior of an SMM.

## 2. Experimental

### 2.1. Syntheses

All procedures were carried out under aerobic conditions and at ambient conditions of temperature and light except for the synthesis of dmhmpH, which was carried out as previously reported [56]. All chemicals were used as received.

#### 2.1.1. $[Gd_4Mn_8O_8(O_2CPh)_{16}(dmhmp)_4]$ (**1**)

To a stirred solution of dmhmpH (0.14 g, 1.0 mmol) in MeCN/MeOH (24/2 mL) was added $Gd(NO_3)_3{\cdot}6H_2O$ (0.23 g, 0.50 mmol) followed by $NEt_3$ (0.52 g, 2.0 mmol). After 10 mins, $Mn(O_2CPh)_2{\cdot}2H_2O$ (0.33 g, 1.0 mmol) was added, the mixture was stirred for a further 2 h, and then it was filtered to remove any undissolved solid. The filtrate was allowed to concentrate at ambient temperature by slow evaporation over 5 days, during which time black crystals of **1**·$^3/_2$MeCN slowly grew. The crystals were collected by filtration, washed with $Et_2O$, and dried under vacuum for 3 h; the yield was 30% based on Mn. The dried solid analyzed as solvent free. *Anal.* Calc. (Found) for **1** ($C_{144}H_{120}O_{44}N_4Mn_8Gd_4$): C, 47.01 (46.93); H, 3.29 (3.29); N, 1.52 (1.60) %. Selected IR data (KBr, $cm^{-1}$): 3460(br), 3065(w), 1600(s), 1557(s), 1410(s), 1178(m), 972(m), 779(m), 718(s), 659(m), 613(m), 559(w), 541(w), 517 (w), 427(m).

#### 2.1.2. $[Tb_4Mn_8O_8(O_2CPh)_{16}(dmhmp)_4]$ (**2**)

The preparation of complex **2** was the same as that for **1** but using $Tb(NO_3)_3{\cdot}5H_2O$ (0.23 g, 0.50 mmol). The yield was 20%. *Anal.* Calc. (Found) for **2** ($C_{144}H_{120}O_{44}N_4Mn_8Tb_4$): C, 46.93 (46.98); H, 3.28 (3.25); N, 1.52 (1.67) %.

#### 2.1.3. $[Dy_4Mn_8O_8(O_2CPh)_{16}(dmhmp)_4]$ (**3**)

The preparation of complex **3** was the same as that for **1** but using $Dy(NO_3){\cdot}5H_2O$ (0.23 g, 0.50 mmol). The yield was 25%. *Anal.* Calc. (Found) for **3** ($C_{144}H_{120}O_{44}N_4Mn_8Dy_4$): C, 46.74 (46.56); H, 3.27 (3.24); N, 1.51 (1.43) %.

#### 2.1.4. $[Ho_4Mn_8O_8(O_2CPh)_{16}(dmhmp)_4]$ (**4**)

The preparation of complex **4** was the same as that for **1** but using $Ho(NO_3){\cdot}5H_2O$ (0.23 g, 0.50 mmol). The yield was 22%. *Anal.* Calc. (Found) for **4** ($C_{144}H_{120}O_{44}N_4Mn_8Ho_4$): C, 46.62 (46.98); H, 3.26 (3.25); N, 1.51 (1.67) %.

#### 2.1.5. $[Y_4Mn_8O_8(O_2CPh)_{16}(dmhmp)_4]$ (**5**)

The preparation of complex **5** was the same as that for **1** but using $Y(NO_3)_3{\cdot}6H_2O$ (0.19 g, 0.50 mmol). The yield of dark-brown crystals of **5**·$^6/_5$MeCN was 25%. Dried solid seemed to be slightly hygroscopic. *Anal.* Calc. (Found) for **5**·$2H_2O$ ($C_{144}H_{124}O_{46}N_4Mn_8Y_4$): C, 50.25 (50.19); H, 3.63 (3.48); N, 1.63 (1.69) %.

### 2.2. X-ray crystallography

X-ray data were collected at 100 K on a Bruker **DUO** diffractometer using Cu Kα radiation ($\lambda$ = 1.54178 Å) from an ImuS power source for **1**·$^3/_2$MeCN, a Bruker **SMART** diffractometer using Mo Kα radiation ($\lambda$ = 0.71073 Å) for **5**·$^6/_5$MeCN, and an APEXII CCD area detector for both. Raw data frames were read by the program SAINT[1] and integrated using 3D profiling algorithms. The resulting data were reduced to produce *hkl* reflections, and their intensities and estimated standard deviations. The data were corrected for Lorentz and polarization effects, and numerical absorption corrections were applied based on indexed and measured faces. The structures were solved and refined on $F^2$ in SHELXTL6.1 using full-matrix least-squares refinement [57]. Non-H atoms were refined with anisotropic thermal parameters, and all H atoms were placed in calculated, idealized positions and refined as riding on their parent atoms.

For **1**·$^3/_2$MeCN, the asymmetric unit consists of half the $Mn_8Gd_4$ cluster and a ¾MeCN solvent molecule. The latter is present only with the major component of the N1 ligand disorder, where the whole ligand is refined in two parts with occupancies of 0.75 and 0.25. Additional disorders are present in Ph groups at C17, C38 and C45, in addition to atom O4 being refined with a minor component, O4′. In the final cycle of refinement, 11577 reflections, of which 8651 were observed with $I > 2\sigma(I)$, were used to refine 859 parameters to give $R_1$, $wR_2$ and $S$ (goodness of fit) of 6.38%, 15.48% and 1.028, respectively.

For **5**·$^6/_5$MeCN, the asymmetric unit consists of half the $Mn_8Y_4$ cluster, and a $^1/_5$ and a $^2/_5$MeCN solvent molecules. The latter are associated with disorder of the N2 and C24 ligands; the whole N2 ligand is disordered and was refined in two parts. The O5 benzoate is disordered and was refined in three parts with their occupancies adding up to one. The O10, O12 and O17 benzoates are also disordered and each was refined in two parts with their occupancies similarly treated. Because of the disorders, atoms C9–C16 and C9′–C16′ were restrained to maintain equivalent site occupation parameters. Similar treatments were applied to disorders including atoms C18–C23, C18′–C23′, C47–C52, and C37′–C52′, and all atoms of the disordered partial solvent molecules. All disordered Ph rings were also constrained to maintain ideal hexagonal geometries. In the final cycle of refinement, 14614 reflections, of which 6858 are observed with $I > 2\sigma(I)$, were used to refine 753 parameters, and the resulting $R_1$, $wR_2$ and $S$ (goodness of fit) were 5.92%,

**Table 1**
Crystallographic and structure refinement data for **1** and **5**.

| | **1**·$^3/_2$MeCN | **5**·$^6/_5$MeCN |
|---|---|---|
| Formula[a] | $C_{147}H_{124.5}Gd_4Mn_8N_{5.5}O_{44}$ | $C_{146.4}H_{123.6}Mn_8N_{5.2}O_{44}Y_4$ |
| FW (g mol$^{-1}$)[a] | 3740.54 | 3454.92 |
| space group | $P\bar{1}$ | $P\bar{1}$ |
| $a$ (Å) | 14.3795(3) | 14.3840(5) |
| $b$ (Å) | 16.2510(3) | 16.3128(6) |
| $c$ (Å) | 16.8160(3) | 16.9181(6) |
| $\alpha$ (°) | 66.631(1) | 65.403(2) |
| $\beta$ (°) | 77.341(1) | 77.640(2) |
| $\gamma$ (°) | 82.177(1) | 82.569(2) |
| V (Å$^3$) | 3514.24(12) | 3522.22(23) |
| $Z$ | 1 | 1 |
| $T$ (K) | 100(2) | 100(2) |
| $\lambda$ (Å) | 0.71073 | 0.71073 |
| $D_{Calc}$ (g cm$^{-1}$) | 1.767 | 1.62872 |
| $\mu$ (mm$^{-1}$) | 18.338 | 2.403 |
| $R_1$[b,c] | 0.0890 | 0.1496 |
| $wR_2$[d] | 0.1796 | 0.1801 |

[a] Including solvent molecules.
[b] $I > 2\sigma(I)$.
[c] $R_1 = \Sigma(||F_o| - |F_c||)/\Sigma|F_o|$.
[d] $wR_2 = [\Sigma[w(F_o^2 - F_c^2)^2]/\Sigma[w(F_o^2)^2]]^{1/2}$.

14.73% and 0.929, respectively. Unit cell data and structure refinement details are listed in Table 1.

### 2.3. Physical measurements

Infrared spectra in the 400–4000 cm$^{-1}$ range were recorded in the solid state (KBr pellets) on a Nicolet Nexus 670 FTIR spectrometer. Elemental analyses (C, H and N) were performed by the in-house facilities of the University of Florida, Chemistry Department. Variable-temperature dc and ac magnetic susceptibility data were collected on a Quantum Design MPMS-XL SQUID magnetometer equipped with a 7 T magnet and operating in the 1.8–300 K range. Samples were embedded in solid eicosane to prevent torquing. Magnetization versus field and temperature data were fit using the program MAGNET [58]. Pascal's constants were used to estimate the diamagnetic corrections, which were subtracted from the experimental susceptibilities to give the molar paramagnetic susceptibility ($\chi_M$). Ultra-low-temperature (<1.8 K) hysteresis and magnetization decay measurements were performed on a single crystal using a micro-SQUID magnetometer [59]. The high sensitivity of this magnetometer allows the study of single crystals of SMMs of the order of 10–500 μm. Crystals were maintained in mother liquor to avoid degradation and were covered in grease for protection during the transfer to the micro-SQUID and subsequent cooling.

## 3. Results and discussion

### 3.1. Syntheses

The oxidation of $Mn^{II}$ benzoate by atmospheric $O_2$ in the presence of a $Ln^{III}$ or $Y^{III}$ nitrate, dmhmpH, and $NEt_3$ in a 2:1:2:4 molar ratio in MeCN/MeOH led to dark brown solutions from which were isolated dark brown or black crystals of the corresponding $[M_4Mn_8O_8(O_2CPh)_{16}(dmhmp)_4]$ (M = Ln or Y) cluster in 20–30% yields. The MeOH was added to ensure solubility of all salts and also led to slightly higher yields and better quality crystals than MeCN alone. The $NEt_3$ was added as a proton acceptor to assist water deprotonation to $O^{2-}$ and to assist aerial oxidation of $Mn^{II}$ by ensuring basic conditions. The reaction for Gd is summarized in Eq. (1). The near-superimposable IR spectra and analytical data indicated **1**–**5** to be isostructural,

$$8Mn(O_2CPh)_2 + 4Gd^{3+} + 4dmhmpH + 2O_2 + 4H_2O \rightarrow [Mn_8Gd_4O_8(O_2CPh)_{16}(dmhmp)_4] + 12H^+ \quad (1)$$

and two representative crystal structures were determined, for **1** (Gd) and **5** (Y), which supported this conclusion.

### 3.2. Description of structures

Complexes **1**·$^3/_2$MeCN and **5**·$^6/_5$MeCN both crystallize in triclinic space group $P\bar{1}$ with the clusters lying on inversion centers. Since the compounds are isostructural, only the structure of **1** will be described in detail here.

The structures of **1** and **5** are shown in Figs. 1 and S1, respectively, and selected core distances and angles are listed in Tables 2 and S1. The $[Mn_8Gd_4(\mu_3\text{-}O^{2-})_4(\mu_4\text{-}O^{2-})_4]$ core can be described as five parallel metal-containing layers in an **ABCBA** pattern (Fig. 1, top), where **A** is Gd, **B** is a $GdMn_2$ triangle, and **C** is a planar $Mn_4$ rhombus. The metals are held together by a combination of four $\mu_3$-$O^{2-}$ and four $\mu_4$-$O^{2-}$ ions, with additional bridges provided by the peripheral organic ligation, which comprises four $\eta^2$:$\eta^1$:μ-dmhmp$^-$ and sixteen $PhCO_2^-$ groups in a variety of binding modes. The latter consist of a chelating $\eta^2$-benzoate on each Gd2 and fourteen bridging benzoates in multiple $\mu_2$ and $\mu_3$ modes; these are shown in Fig. 2, as well as the number of each type in the molecule. The Mn and Gd are six- and nine-coordinate, respectively. The $Mn^{III}$ oxidation states were obvious from the metric parameters and the presence of a clear Jahn–Teller (JT) axial elongation, and they were confirmed by bond valence sum (BVS) calculations (Tables 3, and S2 for **5**) [60,61].

The core can alternatively be described as containing a central $Mn_4$ rhombus that is oxide-bridged to give a $\{Mn_4(\mu_3\text{-}O^{2-})_4(\mu_4\text{-}O^{2-})_2\}$ 'face-fused incomplete double-cubane', a common structural type in tetranuclear Mn/O chemistry [49,62,63], attached on either side to a tetrahedral $\{Gd_2Mn_2(\mu_4\text{-}O^{2-})\}$ unit, as shown in Fig. 1, bottom. The eight O–$Mn^{III}$–O JT elongation axes (Fig. 1, top) separate into multiple sets with different orientations.

The $[Gd_2Mn_8O_8]^{14+}$ core unit comprising the **BCB** layers is very similar to that in homometallic Mn chemistry in the complexes $[Mn_{10}O_8(O_2CPh)_6L_8]$, where L is the anion of picolinic acid or dibenzoylmethane [64]. In these compounds, layer **C** is a $Mn_4$ rhombus

**Table 2**
Selected core interatomic distances (Å) and angles (°) for **1**·$^3/_2$MeCN.[a]

| | |
|---|---|
| Gd1···Gd 23.7593(7) | Mn1···Mn43.408(2) |
| Gd1···Mn 1 3.629(1) | Mn1···Mn4′3.488(2) |
| Gd1···Mn 2 3.508(1) | Mn2···Mn3 3.119(2) |
| Gd2···Mn 1 3.348(1) | Mn3···Mn4 2.905(2) |
| Gd2···Mn 23.399(1) | Mn3···Mn4′ 3.056(2) |
| Mn1···Mn 23.260(2) | Mn4···Mn4′ 3.036(3) |
| Mn1···Mn 33.372(2) | Mn2-O9[b] 2.283(6) |
| Gd1–O22 2.305(5) | Mn2–O12[b] 2.373(7) |
| Gd1–O20 2.397(5) | Mn3–O21 1.891(6) |
| Gd2–O20 2.373(5) | Mn3–O14′ 1.950(7) |
| Mn1–O19 1.864(5) | Mn3–O19 1.975(6) |
| Mn1–O20 1.906(6) | Mn3–O18 2.023(7) |
| Mn1–O2 1.915(6) | Mn3–O22′ 2.023(6) |
| Mn1–N2 2.032(8) | Mn3–O12[b] 2.231(8) |
| Mn1–O11[b] 2.218(7) | Mn4–O22 1.880(6) |
| Mn1–O16[b] 2.287(6) | Mn4–O19′ 1.900(6) |
| Mn2–O21 1.870(5) | Mn4–O21 1.924(6) |
| Mn2–O20 1.880(6) | Mn4–O15′1.986(6) |
| Mn2–O1 1.908(6) | Mn4–O10[b] 2.240(6) |
| Mn2–N1′ 1.95(3) | Mn4–O22′[b] 2.272(6) |
| Mn2–N1 2.044(11) | |

[a] Primed and unprimed atoms are related by symmetry.
[b] $Mn^{III}$ Jahn-Teller elongation axis.

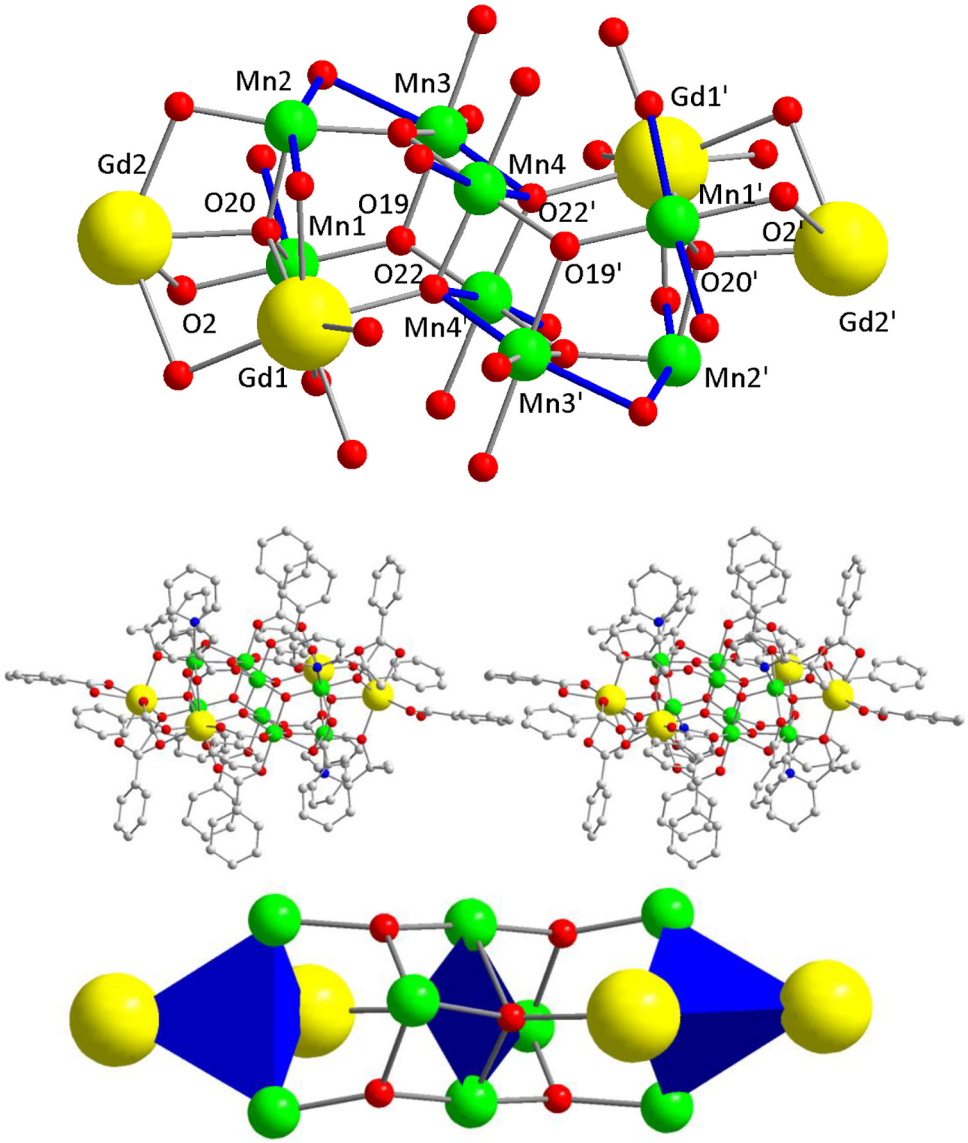


**Fig. 1.** (top) Partially-labeled core of centrosymmetric **1** with the $Mn^{III}$ JT elongation axes shown as blue Mn-O bonds; (middle) a stereopair of the complete molecule, with H atoms omitted for clarity; and (bottom) the core emphasizing the two $Gd_2Mn_2$ tetrahedra either side of the central $Mn_4$ rhombus. Color code: Gd yellow, Mn green, O red, N blue, C grey. (Color online.)

and the **B** layers comprise $Mn_3$ triangular units. In heterometallic chemistry, an $[Ln_2Mn_{10}]$ SMM family from the use of 2-hydroxymethylpyridine (hmpH) has also been reported to possess five **ABCBA** layers [20], corresponding to the homometallic $Mn_{10}$ structure plus a Ln ion attached at each end. The $[Ln_2Mn_{10}]$ and present $[Ln_4Mn_8]$ families from hmpH and dmhmpH, respectively, are overall structurally similar, except for the Ln:Mn composition and resulting differences in bond distances and angles. There is one previous $[Mn_8Ln_4]$ family in the literature with an overall similar structure to **1**–**5** but with a different formulation of $[Ln_4Mn_8O_8(O_2CPh)_{12}(hmp)_4(NO_3)_4(PhCO_2H)(EtOH)]$ and a different, less symmetric means of attachment of the end Ln ions [33].

The packing diagram for **1** reveals many weak intermolecular C–H···C contacts, as expected for large clusters with organic ligands. The partial-occupancy MeCN solvent molecules weakly bridge two adjacent clusters by forming N···H–C hydrogen-bonds (3.43(5) Å) to a Ph group of one cluster and C–H···O hydrogen-bonds (3.50(5) Å) to atom O(4) of the chelating benzoate on Gd (2) in the neighboring cluster.

### 3.3. Magnetochemistry

#### 3.3.1. Dc magnetic susceptibility studies

Solid-state, variable-temperature magnetic susceptibility measurements were performed on powdered microcrystalline samples in the 5.0–300 K range and in a 1 kG (0.1 T) dc field. The samples were restrained in eicosane to prevent torquing. The obtained data are presented as $\chi_M T$ versus $T$ plots in Fig. 3, and selected data are listed in Table 4.

For **5**·$2H_2O$, which contains diamagnetic $Y^{III}$ ions, $\chi_M T$ decreases from 31.2 $cm^3$ K $mol^{-1}$ at 300 K to a near-plateau below ~20 K and a value of 12.4 $cm^3$ K $mol^{-1}$ at 5.0 K. $\chi_M T$ at 300 K is larger than the spin-only ($g = 2$) value calculated for eight non-interacting $Mn^{III}$ ions of 24.0 $cm^3$ K $mol^{-1}$ (Table 4), indicating both ferromagnetic (**F**) and antiferromagnetic (**AF**) interactions within the $Mn_8$ unit; the presence of **F** interactions is not surprising given that this is commonly encountered in discrete $Mn_4$ complexes with the 'face-fused incomplete double-cubane' core topology [18,49,62,63]. The $\chi_M T$ at 5.0 K and the near-plateau below ~20 K

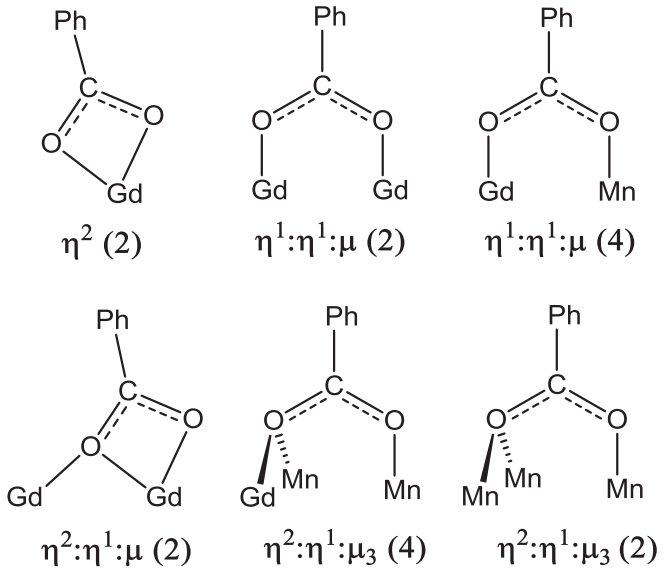


**Fig. 2.** The different benzoate binding modes in **1**. The numbers in parentheses are the number of such ligands in the molecule.

**Table 3**
BVS calculations for the Mn atoms in complex **1**.[a]

| Atom | $Mn^{II}$ | $Mn^{III}$ | $Mn^{IV}$ |
|---|---|---|---|
| Mn1 | 3.26 | 3.01 | 3.13 |
| Mn2 | 3.36 | 3.19 | 3.27 |
| Mn3 | 3.18 | 2.91 | 3.08 |
| Mn4 | 3.13 | 2.86 | 3.03 |

[a] The oxidation state of a particular Mn is the nearest integer to the underlined value, which is the closest to the charge for which it was calculated.

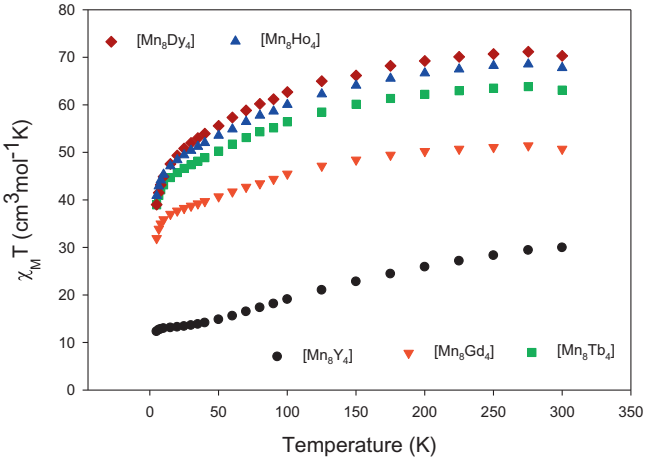


**Fig. 3.** $\chi_M T$ vs $T$ plots for complexes **1**–**4** and **5**·2$H_2O$ in a 1 kG (0.1 T) dc field.

suggest a fairly well isolated $S = 5$ ground state for **5**, which would be surprising for such a high nuclearity cluster (vide infra).

For **1**, which contains isotropic $Gd^{III}$ ions with $S = {}^7/_2$, $\chi_M T$ gradually decreases from 51.2 $cm^3$ K $mol^{-1}$ at 300 K to 38.8 $cm^3$ K $mol^{-1}$ at 20.0 K and then decreases more rapidly to 31.5 $cm^3$ K $mol^{-1}$ at 5.0 K. The $\chi_M T$ at 300 K is now slightly smaller than the spin-only value of 55.5 $cm^3$ K $mol^{-1}$ for a non-interacting $Gd_4Mn_8$ system, suggesting small changes to the constituent $J$ values compared with **5** caused by the Gd-for-Y substitution. The steeper decrease at the lowest $T$ suggests the Gd···Mn coupling is dominantly **AF**. We note that Gd ions are interacting with Mn ions in both layers **B** and **C**, and will discuss the likely effect of this below.

For **2**–**4**, which contain anisotropic $Ln^{III}$ ions, the $\chi_M T$ at 300 K are 65.1, 71.0 and 68.7 $cm^3$ K $mol^{-1}$, respectively, which like **1** are all slightly less than calculated for eight $Mn^{III}$ and four $Ln^{III}$ non-interacting ions with $g = 2$. They then decease steadily with decreasing $T$ (Fig. 3) and, again as for **1**, the decrease accelerates at the lowest temperatures reaching 34.6, 38.8, and 40.8 $cm^3$ K $mol^{-1}$, respectively, suggesting dominant **AF** Ln···Mn coupling. Since the $\chi_M T$ for **5**·2$H_2O$ is essentially a plateau below ~20 K, it cannot be responsible for the low $T$ decreases for **1**–**4**, which are instead assigned to the weak Mn···Ln coupling.

### 3.3.2. Ac magnetic susceptibility studies

Ac susceptibility data for complexes **1**–**4** and **5**·2$H_2O$ were collected in the 1.8–15 K range using a 3.5 Oe ac field oscillating at frequencies in the 50–1000 Hz range. The obtained in-phase ac susceptibility ($\chi'_M$) data at 1000 Hz for all the complexes are shown as $\chi'_M T$ versus $T$ in Fig. 4. For the $Y^{III}$ analogue **5**·2$H_2O$, $\chi'_M T$ is almost temperature-independent below 15 K at ~13 $cm^3$ K $mol^{-1}$, exhibiting only a slight decrease with decreasing $T$, similar to the behavior seen in the dc plot (Fig. 3). For **1**, containing isotropic $Gd^{III}$ ($S = {}^7/_2$), $\chi'_M T$ steadily decreases from 38.4 $cm^3$ K $mol^{-1}$ at 15 K to 22.6 $cm^3$ K $mol^{-1}$ at 1.8 K. This behavior is consistent with depopulation of the many low-lying excited states from the very weak exchange coupling expected between the $Gd^{III}$ ions and the $Mn_8$ unit. This overall decreasing $\chi'_M T$ at the lowest $T$ supports the conclusions from the dc studies above that the dominant Gd···Mn exchange coupling is **AF**. Similar profiles are obtained for **2**–**4** containing anisotropic $Tb^{III}$, $Dy^{III}$, and $Ho^{III}$, respectively, all exhibiting a decreasing $\chi'_M T$ with decreasing $T$. This is again consistent with dominant **AF** Ln..Mn exchange coupling, i.e., if there are any **F** Ln···Mn interactions, they are weaker than the **AF** ones.

Examination of the $\chi'_M T$ versus $T$ plots for **1**–**5** in the 50–1000 Hz ac frequency range reveals that only **3** exhibits a noticeable frequency-dependence down to 1.8 K and concomitant strong out-of-phase ($\chi''_M$) signals (Fig. 5) suggestive of the slow magnetization relaxation of a SMM. The other compounds show essentially no frequency-dependent $\chi'_M T$ or $\chi''_M$ signals (Figs. S2–S5) down to 1.8 K.

One interpretation of the near-$T$-independent data for **5**·2$H_2O$ is that they arise from a well-isolated $S = 5$ ground state with $g < 2$, as expected for a $Mn^{III}$-containing cluster; the spin-only ($g = 2$) $\chi'_M T$ for $S = 4$, 5 and 6 systems is 10.0, 15.0, and 21.0 $cm^3$ K $mol^{-1}$, respectively. However, the $\chi'_M T$ of only ~13 $cm^3$ K $mol^{-1}$ would suggest $g$ ~1.86, rather smaller than the 1.95–2.00 range normally expected for $Mn^{III}$. Moreover, a well-isolated single ground state spin for such a high nuclearity $Mn_8^{III}$ cluster is unusual, as already mentioned above, since some of the pairwise $Mn_2^{III}$ exchange interactions are likely very weak and will lead to at least some very low-lying excited states. These combined points thus made us consider instead the possibility that one or more excited states were essentially degenerate with the ground state, leading to a $\chi'_M T$ that changes little at these low temperatures because the Boltzmann populations are almost constant. For example, exactly degenerate $S = 4$ and $S = 5$ states would give $\chi'_M T = 12.8$ $cm^3$ K $mol^{-1}$, consistent with Fig. 6. To probe this possibility further, we thus decided to carry out additional dc studies.

### 3.3.3. Dc magnetization fits

Magnetization ($M$) data were collected at dc fields ($H$) up to 7 T in the 1.8–10 K range. For a single well-isolated ground state spin $S$, we typically obtain very good fits of the resulting $M/N\mu_B$ versus $H/T$ data, where $N$ is Avogadro's number and $\mu_B$ is the Bohr magneton,

**Table 4**
Selected magnetic data for complexes **1**–**5**.[a]

| Compounds | Ln/Y free ion term | $\chi_M T$[a] Ln/Y free ion | $\chi_M T$[a] exptl 5 K | $\chi_M T$[a] exptl 300 K | $\chi_M T$[a,b] calc |
|---|---|---|---|---|---|
| $[Mn_8Gd_4]$ (**1**) | $^8S_{7/2}$ | 7.9 | 31.5 | 51.2 | 55.6 |
| $[Mn_8Tb_4]$ (**2**) | $^7F_6$ | 11.8 | 34.6 | 65.1 | 71.2 |
| $[Mn_8Dy_4]$ (**3**) | $^6H_{15/2}$ | 14.2 | 38.8 | 71.0 | 80.8 |
| $[Mn_8Ho_4]$ (**4**) | $^5I_8$ | 14.1 | 40.8 | 68.7 | 80.4 |
| $[Mn_8Y_4]$ (**5**) | $^1S_0$ | 0 | 12.4 | 31.2 | 24.0 |

[a] Units: $cm^3\ K\ mol^{-1}$.
[b] Calculated for non-interacting $Mn_8^{III}Ln_4^{III}$ or $Mn_8^{III}Y_4^{III}$ ions with $g = 2$.

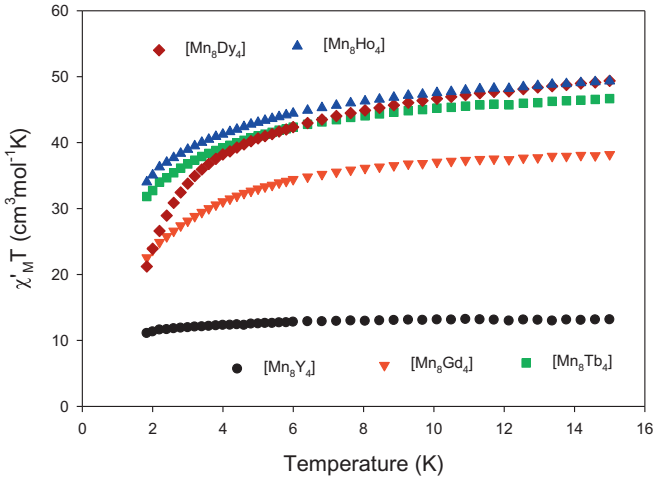


**Fig. 4.** The in-phase ac susceptibility $\chi'_M T$ signals at 1000 Hz for **1** (Gd), **2** (Tb), **3** (Dy), **4** (Ho) and **5**·2H$_2$O (Y) in the 1.8–15 K range. The solid lines are guides to the eye.

using the program MAGNET [56]. This diagonalizes the spin Hamiltonian matrix assuming only the ground state is populated, includes axial anisotropy ($D\hat{S}_z^2$) and the Zeeman effect, and employs a full powder average. The corresponding spin Hamiltonian is given in Eq. (2), where $\hat{S}_z$ is the z-axis spin operator, and $\mu_o$ is the vacuum permeability.

$$H = D\hat{S}_z^2 + g\mu_B\mu_o\hat{S}\cdot H \quad (2)$$

In contrast to what is normally found for well-isolated ground states, however, we could not get any acceptable fit for **5**·2H$_2$O using all the data. Progressively excluding more and more of the data collected at low fields (a common way of removing complications from intermolecular interactions) or at high fields (to remove complications from low-lying excited states with $S$ greater than that of the ground state) also gave poor fits; in any case, the crystal structure shows no significant intermolecular interactions (vide supra). Only when data just at the highest fields (4–7 T) were employed was even a somewhat reasonable fit achieved, with fit parameters of $S = 5$, $g = 1.97(2)$, and $D = -0.81(4)\ cm^{-1}$ (Fig. 6). Also omitting data above 4 K gave no significant improvement in the fit (Fig. S6). We interpret these observations as indicating that **5**·2H$_2$O has two or more near-degenerate $S$ states at the ground state, with the one with the largest spin being $S = 5$, and thus only at high applied fields are the components of the $S = 5$ state sufficiently stabilized in energy and separated from those of the smaller spin states (such as $S = 4$) to permit even a fair fit to a single spin state to be achieved. We thus conclude that **5**·2H$_2$O indeed does not have a well-isolated singly-degenerate ground state, which is consistent with its high $Mn_8^{III}$ nuclearity. For **2**–**4**, no reasonable fits could be obtained using any data, consistent with the extra complication of many low-lying excited states from weak Mn..Ln coupling.

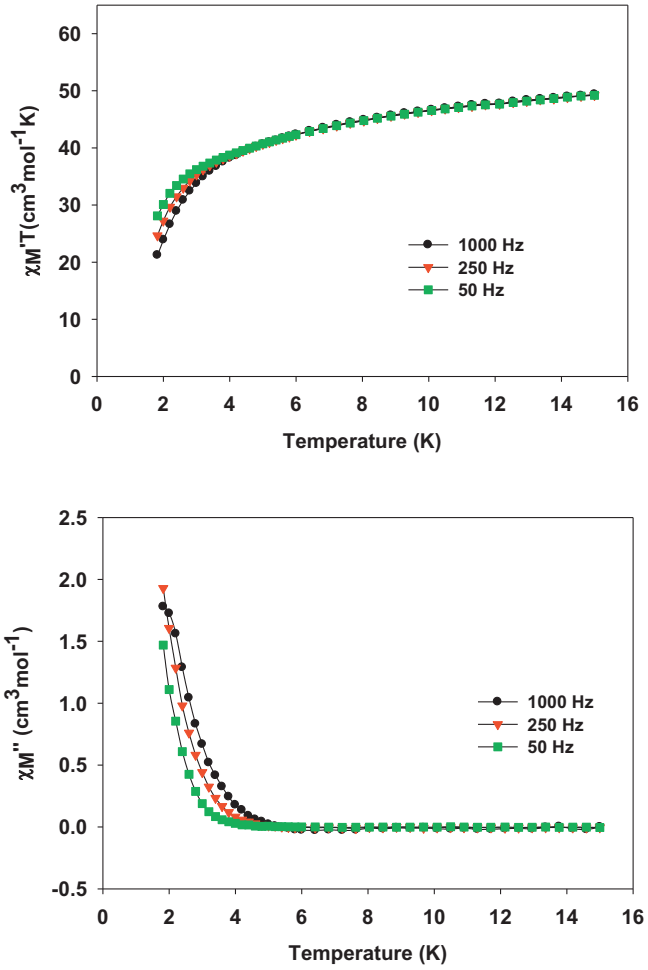


**Fig. 5.** In-phase ($\chi'_M$, as $\chi'_M T$) (top) and out-of-phase ($\chi''_M$) (bottom) ac susceptibility signals vs $T$ plots for **3** in the 1.8–15 K range. The solid lines are guides to the eye.

### 3.3.4. $[Gd_4Mn_8O_8(O_2CPh)_{16}(dmhmp)_4]$ (**1**) versus $[Gd_2Mn_{10}O_8(O_2CPh)_{10}(hmp)_6(NO_3)_4]$

The core structure of the present $[Ln_4Mn_8O_8(O_2CPh)_{16}(dmhmp)_4]$ family is similar to that of the recently reported $[Ln_2Mn_{10}O_8(O_2CPh)_{10}(hmp)_6(NO_3)_4]$ family [20]. Both contain an **ABCBA** layered structure with a $Ln^{III}$ (or $Y^{III}$) ion occupying each layer **A**. However, a big difference between the families is that **1**–**5** also have one additional $Ln^{III}$ (or $Y^{III}$) ion in each layer **B** giving a $LnMn_2$ triangular unit rather than a $Mn_3$ one. As a result, there are

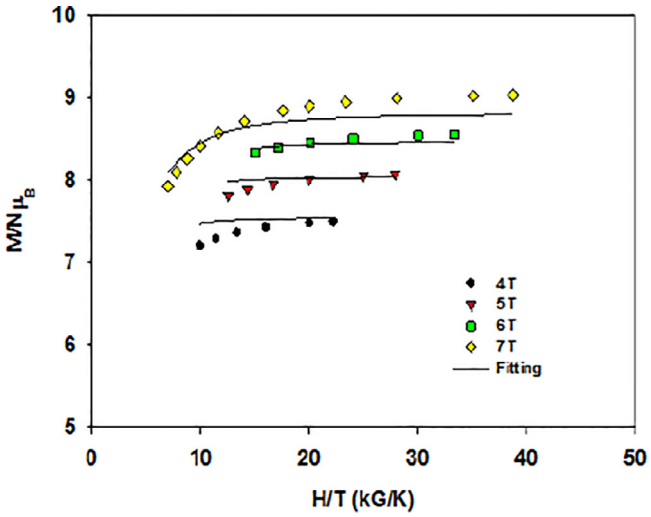


**Fig. 6.** Reduced magnetization ($M/N\mu_B$) vs $H/T$ plots for **5** at applied fields of 4.0–7.0 T in the 1.8–10 K temperature range. The solid lines are the fit of the data; see the text for the fit parameters.

two distinctly different types of Ln. . .Mn exchange couplings in **1**–**4**, which will be described using representative complex **1** (Fig. 1): (i) Gd2 in layer **A** couples to Mn1 and Mn2 in layer **B** via the $\mu_4$-$O^{2-}$ ion O20 (Gd2–O20 = 2.373(5) Å); and (ii) Gd1 in layer **B** couples to Mn1 and Mn2 in the same layer through O20 (Gd1–O20 = 2.397(5) Å), but also to Mn3′, Mn4 and Mn4′ in layer **C** through $\mu_4$-$O^{2-}$ ion O22 (Gd1–O22 = 2.305(5) Å). Only the first type (i) is present in the $\{Ln_2Mn_{10}\}$ family. Point (ii) suggests that Gd1 in **1** is coupled more strongly to the $Mn_8$ fragment than Gd2. This helps to rationalize some obvious differences in the magnetic properties of the two families, especially the fact that **1**–**4** all show dominant **AF** Ln..Mn couplings, whereas some of the $\{Ln_2Mn_{10}\}$ family, with Ln = Tb and Dy, exhibit **F** Ln. . .Mn coupling [20]. Even if the corresponding Tb and Dy complexes **2** and **3** also had **F** couplings with Gd2 in layer **A**, the stronger **AF** couplings with Gd1 would give an overall dominant **AF** coupling between the $Mn_8$ and Ln ions.

*3.3.5. Single-crystal hysteresis studies below 1.8 K*

In order to probe further the possible SMM nature of **3**, magnetization versus dc field scans for a single crystal were carried out at various temperatures and scan rates. The resultant data (Fig. 7) display hysteresis loops below a blocking temperature ($T_B$) of 1.6 K whose coercivity increases with decreasing $T$ and increasing scan rate, as expected for an SMM. No QTM steps are seen, except poorly-defined shoulders at some positions, which is completely consistent with the high nuclearity of **3** and its many very low-lying excited states.

The large coercivity below 0.3 K at $M/M_S = 0$ of ~0.75 T is noteworthy and in stark contrast with that in the hysteresis loop of $[Dy_2Mn_{10}O_8(O_2CPh)_{10}(hmp)_6(NO_3)_4]$ [20] at the same $T$ and scan rate (Fig. S7), which shows a coercivity under the same conditions of only ~0.1 T due to a large QTM step at zero field. We assign this difference to the presence in **3** of two $Dy^{III}$ ions in layer **B** and thus being more strongly coupled to the $Mn_8$ unit, as described above, and decreasing the QTM at zero field, although the exact mechanism of this is unclear.

We did not carry out a magnetization decay study to obtain an Arrhenius plot since **3** is only a weak SMM. Instead we estimated the approximate effective barrier ($U_{eff}$) to magnetization relaxation by employing the Kramers–Kronig equation of Eq. (3) [65], where $\tau_0$ is the Arrhenius pre-

$$\ln(\chi''/\chi') = \ln(\omega\tau_0) + \Delta/k_bT \quad (3)$$

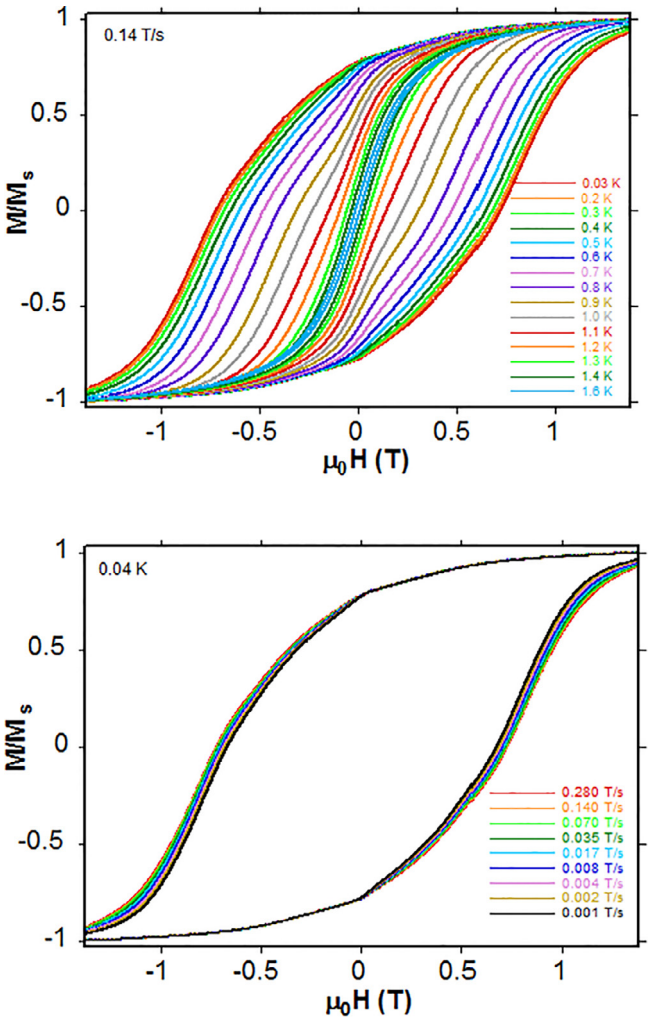


**Fig. 7.** Magnetization ($M$) vs. dc field hysteresis loops for a single crystal of **3** at the indicated temperatures with a 0.14 T/s scan rate (top), and the indicated scan rates at 0.04 K (bottom). The magnetization is normalized to its saturation value, $M_S$.

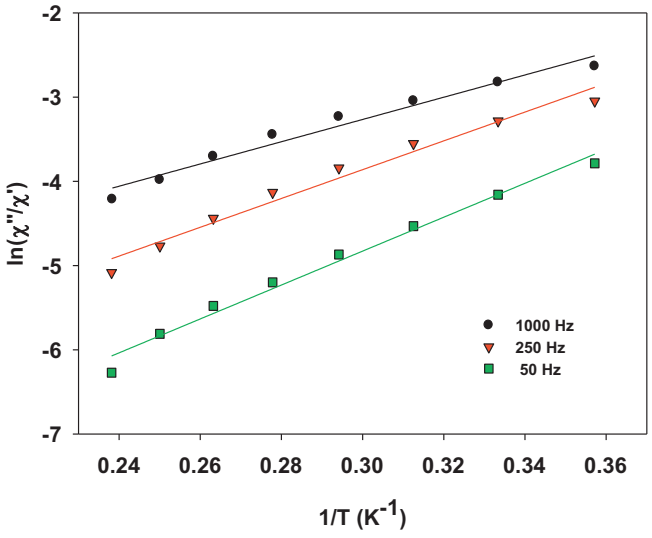


**Fig. 8.** Plot of $\ln(\chi''_M/\chi'_M)$ vs $1/T$ for **3** at the indicated frequencies. The solid lines are the fit; see the text for the fit parameters.

exponential factor, $k$ is the Boltzmann constant, and ω is the ac oscillation frequency. The resulting data and their fit to Eq. (3) are shown in Fig. 8, and the fit parameters were $U_{eff} = 12(1)\ cm^{-1}$ and $\tau_0 = 9(2) \times 10^{-8}$ s. The small $U_{eff}$ is fully consistent with the $\chi''$ versus $T$ plot, which shows signals only at very low $T$.

## 4. Conclusions

The air-oxidation of $Mn(O_2CPh)_2{\cdot}4H_2O$ in the presence of $Y^{III}$ or $Ln^{III}$ salts and dmhmpH has proven a convenient route to the $\{Y_4Mn_8\}$ and $\{Ln_4Mn_8\}$ complexes **1**–**5**. The $dmhmp^-$ ligand and its $CMe_2$ rather than $CH_2$ next to the alkoxide O atom has thus led to a similar but nevertheless distinctly different product than we obtained with $hmp^-$, i.e., $[Ln_4Mn_8O_8(O_2CPh)_{16}(dmhmp)_4]$ versus $[Ln_2Mn_{10}O_8(O_2CPh)_{10}(hmp)_6(NO_3)_4]$. The two extra Ln ions in **1**–**4** occur in layer **B** and seem to couple with the $Mn_8$ fragment more strongly than those in layer **A** do. The Dy analog **3** has been confirmed as a SMM by the observation of hysteresis loops below a blocking temperature ($T_B$) of 1.6 K in a micro-SQUID study. To complete this study, the bulkier derivative of hmpH with a $CPh_2$ unit next to the O atom, namely dphmpH, has also been employed in Ln/Mn cluster chemistry, and the results of this study will be reported in due course.

## Acknowledgement

This work was supported by the USA National Science Foundation (CHE-1565664).

## Appendix A. Supplementary data

CCDC 1815941 and 1815942 contains the supplementary crystallographic data for **1**·$^3/_2$MeCN and **5**·$^6/_5$MeCN, respectively. These data can be obtained free of charge via http://www.ccdc.cam.ac.uk/conts/retrieving.html, or from the Cambridge Crystallographic Data Centre, 12 Union Road, Cambridge CB2 1EZ, UK; fax: (+44) 1223-336-033; or e-mail: deposit@ccdc.cam.ac.uk. Supplementary data associated with this article can be found, in the online version, at https://doi.org/10.1016/j.poly.2018.07.007.

## References

[1] M.G. Kanatzidis, R. Pöttgen, W. Jeitschko, Angew. Chem. Int. Ed. Engl. 44 (2005) 6996.
[2] S. Osa, T. Kido, N. Matsumoto, N. Re, A. Pochaba, J. Mrozinski, J. Am. Chem. Soc. 126 (2004) 420.
[3] T. Taguchi, M. Thompson, K. Abboud, G. Christou, Dalton Trans. 39 (2010) 9131.
[4] A. Mishra, W. Wernsdorfer, S. Parsons, G. Christou, E.K. Brechin, Chem. Commun. (2005) 2086.
[5] C. Papatriantafyllopoulou, K.A. Abboud, G. Christou, Inorg. Chem. 50 (2011) 8959.
[6] C.G. Efthymiou, T.C. Stamatatos, C. Papatriantafyllopoulou, A.J. Tasiopoulos, W. Wernsdorfer, S.P. Perlepes, G. Christou, Inorg. Chem. 49 (2010) 9737.
[7] Y.-F. Zeng, G.-C. Xu, X. Hu, Z. Chen, X.-H. Bu, S. Gao, E.C. Sañudo, Inorg. Chem. 49 (2010) 9734.
[8] M. Hołyńska, D. Premužić, I.-R. Jeon, W. Wernsdorfer, R. Clérac, S. Dehnen, Chem. Eur. J. 17 (2011) 9605.
[9] H.Z. Kou, S. Gao, X. Jin, Inorg. Chem. 40 (2001) 6295.
[10] J.P. Costes, F. Dahan, W. Wernsdorfer, Inorg. Chem. 45 (2005) 5–7.
[11] M. Estrader, J. Ribas, V. Tangoulis, X. Solans, M. Font-Bardía, M. Maestro, C. Diaz, Inorg. Chem. 45 (2006) 8239.
[12] X.-Q. Zhao, J. Wang, D.-X. Bao, S. Xiang, Y.-J. Liu, Y.-C. Li, Dalton Trans. 46 (2017) 2196–2203.
[13] H. Han, X. Li, X. Zhu, G. Zhang, S. Wang, X. Hang, J. Tang, W. Liao, Eur. J. Inorg. Chem. 2017 (2017) 2088–2093.
[14] M.A. Bolcar, S.M.J. Aubin, K. Folting, D.N. Hendrickson, G. Christou, J. Chem. Soc., Chem. Commun. (1997) 1485.
[15] L. Pham, K.A. Abboud, W. Wernsdorfer, G. Christou, Polyhedron 66 (2013) 205–211.
[16] A.B. Canaj, D.A. Kalofolias, M. Siczek, T. Lis, R. McNab, G. Lorusso, R. Inglis, M. Evangelisti, C.J. Milios, Dalton Trans. 46 (2017) 3449–3452.
[17] M. Sakamoto, T. Ishikawa, Y. Nishida, Y. Sadaoka, A. Matsumoto, Y. Fukuda, M. Sakai, M. Ohba, H. Sakiyama, H. Ōkawa, J. Alloys Compd. 238 (1996) 23–27.
[18] A. Saha, M. Thompson, K.A. Abboud, W. Wernsdorfer, G. Christou, Inorg. Chem. 50 (2011) 10476.
[19] G. Karotsis, S. Kennedy, S.J. Teat, C.M. Beavers, D.A. Fowler, J.J. Morales, M. Evangelisti, S.J. Dalgarno, E.K. Brechin, J. Am. Chem. Soc 132 (2010) 12983–12990.
[20] R. Bagai, W. Wernsdorfer, K. Abboud, G. Christou, Polyhedron 142 (2018) 49–57.
[21] A. Mishra, W. Wernsdorfer, K.A. Abboud, G. Christou, J. Am. Chem. Soc 126 (2004) 15648–15649.
[22] C.M. Zaleski, E.C. Depperman, J.W. Kampf, M.L. Kirk, V.L. Pecoraro, Angew. Chem. Int. Ed. Engl. 43 (2004) 3912–3914.
[23] V.M. Mereacre, A.M. Ako, R. Clérac, W. Wernsdorfer, G. Filoti, J. Bartolomé, C.E. Anson, A.K. Powell, J. Am. Chem. Soc 129 (2007) 9248–9249.
[24] T.C. Stamatatos, S.J. Teat, W. Wernsdorfer, G. Christou, Angew. Chem. Int. Ed. Engl. 48 (2009) 521–524.
[25] A.M. Ako, V. Mereacre, R. Clerac, W. Wernsdorfer, I.J. Hewitt, C.E. Anson, A.K. Powell, Chem. Commun. (2009) 544.
[26] C. Papatriantafyllopoulou, W. Wernsdorfer, K.A. Abboud, G. Christou, Inorg. Chem. 50 (2011) 421.
[27] H. Chen, C.-B. Ma, M.-Q. Hu, H.-M. Wen, H.-H. Cui, J.-Y. Liu, X.-W. Song, C.-N. Chen, Dalton Trans. 42 (2013) 4908.
[28] J.-L. Liu, W.-Q. Lin, Y.-C. Chen, J.-D. Leng, F.-S. Guo, M.-L. Tong, Inorg. Chem. 52 (2012) 457.
[29] V. Mereacre, Y. Lan, W. Wernsdorfer, C.E. Anson, A.K. Powell, C. R. Chimie 15 (2012) 639.
[30] J.-L. Liu, W.-Q. Lin, Y.-C. Chen, J.-D. Leng, F.-S. Guo, M.-L. Tong, Inorg. Chem. 52 (2013) 457.
[31] P. Bag, A. Chakraborty, G. Rogez, V. Chandrasekhar, Inorg. Chem. 53 (2014) 6524.
[32] H. Chen, C.-B. Ma, M.-Q. Hu, H.-M. Wen, C.-N. Chen, Dalton Trans. 43 (2014) 16737.
[33] L. Sun, H. Chen, C. Ma, C. Chen, Dalton Trans. 44 (2015) 20964.
[34] X.-L. Li, F.-Y. Min, C. Wang, S.-Y. Lin, Z. Liu, J. Tang, Dalton Trans. 44 (2015) 3430.
[35] L. Sun, H. Chen, C. Ma, C. Chen, Inorg. Chem. Commun. 70 (2016) 132.
[36] L. Sun, H. Chen, C. Ma, C. Chen, Inorg. Chem. Commun. 77 (2017) 77.
[37] M.N. Leuenberger, D. Loss, Nature 410 (2001) 789.
[38] W. Wernsdorfer, R. Sessoli, Science 284 (1999) 133.
[39] T.N. Nguyen, W. Wernsdorfer, K.A. Abboud, G. Christou, J. Am. Chem. Soc 133 (2011) 20688.
[40] S. Hill, R.S. Edwards, N. Aliaga-Alcalde, G. Christou, Science 302 (2003) 1015.
[41] W. Wernsdorfer, N. Aliaga-Alcalde, D.N. Hendrickson, G. Christou, Nature 416 (2002) 406.
[42] T.N. Nguyen, W. Wernsdorfer, M. Shiddiq, K.A. Abboud, S. Hill, G. Christou, Chem. Sci. 7 (2016) 1156.
[43] F.-S. Guo, B.M. Day, Y.-C. Chen, M.-L. Tong, A. Mansikkamäki, R.A. Layfield, Angew. Chem. Int. Ed. 56 (2017) 11445.
[44] C. Goodwin, F. Ortu, D. Reta, N. Chilton, D. Mills, Nature 548 (2017) 439.
[45] N.C. Harden, M.A. Bolcar, W. Wernsdorfer, K.A. Abboud, W.E. Streib, G. Christou, Inorg. Chem. 42 (2003) 7067.
[46] C. Boskovic, E.K. Brechin, W.E. Streib, K. Folting, J.C. Bollinger, D.N. Hendrickson, G. Christou, J. Am. Chem. Soc. 124 (2002) 3725.
[47] T.C. Stamatatos, K.A. Abboud, W. Wernsdorfer, G. Christou, Angew. Chem. Int. Ed. Engl. 45 (2006) 4134.
[48] M. Bolcar, S. Aubin, K. Folting, D. Hendrickson, G. Christou, Chem. Commun. (1997) 1485.
[49] T. Taguchi, M.R. Daniels, K.A. Abboud, G. Christou, Inorg. Chem. 48 (2009) 9325.
[50] T. Taguchi, W. Wernsdorfer, K.A. Abboud, G. Christou, Inorg. Chem. 49 (2010) 10579.
[51] T. Taguchi, W. Wernsdorfer, K.A. Abboud, G. Christou, Inorg. Chem. 49 (2009) 199.
[52] A. Mishra, A.J. Tasiopoulos, W. Wernsdorfer, K.A. Abboud, G. Christou, Inorg. Chem. 46 (2007) 3105.
[53] J. Feuersenger, D. Prodius, V. Mereacre, R. Clérac, C.E. Anson, A.K. Powell, Inorg. Chem. Commun. 14 (2011) 1851.
[54] C. Papatriantafyllopoulou, K.A. Abboud, G. Christou, Polyhedron 52 (2013) 196.
[55] L. Sun, H. Chen, C. Ma, C. Chen, RSC Adv. 6 (2016) 12408.
[56] N.I. Tzerpos, A.K. Zarkadis, R.P. Kreher, L. Repas, M. Lehnig, J. Chem. Soc. Perkin Trans. 2 (1995) 755.
[57] SHELXTL6, Bruker-AXS, Madison, Wisconsin, USA, 2000.
[58] E.R. Davidson, MAGNET, Indiana University, Bloomington, IN, 1999.
[59] W. Wernsdorfer, Adv. Chem. Phys. (2001) 99.
[60] N.E.B.A.M. O'Keeffe., Acta Crystallogr., Sect. B 47 (1991) 192.
[61] G.J. Palenik, Inorg. Chem. 36 (1997) 4888.
[62] M.D. Godbole, O. Roubeau, A.M. Mills, H. Kooijman, A.L. Spek, E. Bouwman, Inorg. Chem. 45 (2006) 6713.
[63] A. Igashira-Kamiyama, T. Kajiwara, M. Nakano, T. Konno, T. Ito, Inorg. Chem. 48 (2009) 11388.
[64] H.J. Eppley, S.M.J. Aubin, W.E. Streib, J.C. Bollinger, D.N. Hendrickson, G. Christou, Inorg. Chem. 36 (1997) 109.
[65] J. Bartolomé, G. Filoti, V. Kuncser, G. Schinteie, V. Mereacre, C.E. Anson, A.K. Powell, D. Prodius, C. Turta, Phys. Rev. B 80 (2009) 014430.